Open access • Journal Article • DOI:10.1016/J.IJROBP.2018.06.038

Radiation-Induced Lung Density Changes on CT Scan for NSCLC : No Impact of Dose-Escalation Level or Volume — Source link

Gilles Defraene, Matthew D. La Fontaine, Simon van Kranen, Bart Reymen ...+3 more authors

Institutions: Katholieke Universiteit Leuven, Netherlands Cancer Institute, Maastricht University

Published on: 01 Nov 2018 - International Journal of Radiation Oncology Biology Physics (Elsevier Science)

Topics: Standardized uptake value and Hounsfield scale

*Title Page (WITH Author Details)

TITLE:

Radiation-induced lung density changes on CT scan for NSCLC: no impact of dose-escalation level or volume

SHORT TITLE:

Dose-escalation has no impact on lung damage

AUTHORS:

Gilles Defraene[1], Matthew La Fontaine[2], Simon van Kranen[2], Bart Reymen[3], José Belderbos[2], Jan-Jakob Sonke[2], Dirk De Ruysscher[1,3]

AFFILIATIONS:

[1]KU Leuven - University of Leuven, Department of Oncology, Experimental Radiation Oncology, B-3000 Leuven, Belgium

[2]Department of Radiation Oncology, Netherlands Cancer Institute, Amsterdam, The Netherlands

[3] Maastricht University Medical Center+, Department of Radiation Oncology (Maastro clinic), GROW School for Developmental Biology and Oncology, Maastricht, The Netherlands

AUTHOR RESPONSIBLE FOR STATISTICAL ANALYSES:

Gilles Defraene[1]

CORRESPONDING AUTHOR:

Gilles Defraene, PhD

KU Leuven - University of Leuven, Department of Oncology, Experimental Radiation Oncology, B-3000 Leuven, Belgium

Telephone: 32 16 34 01 21

Fax: 32 16 34 76 10

e-mail: gilles.defraene@uzleuven.be

TOTAL FIGURES: 3

TOTAL TABLES: 3

CONFLICT OF INTEREST STATEMENT:

Nothing to disclose.

ACKNOWLEDGEMENTS:

This project has received funding from the European Union's Seventh Framework Programme for research, technological development and demonstration under grant agreement no 257144 (ARTFORCE) and no 601826 (REQUITE).

All authors have approved the final version of the article.

Abstract

Purpose

Dose-escalation for NSCLC patients within the PET-boost trial (NCT01024829) exposes portions of normal lung tissue to high radiation doses. The relationship between lung parenchyma dose and density changes on CT was analyzed.

Methods and Materials

CT scans of 59 stage IB-III NSCLC patients, randomized between a boost to the whole primary tumor and an integrated boost to its 50% SUV_{max} volume, were analyzed in this study. Patients were treated with concurrent or sequential chemoradiation or radiation only. Deformable registration mapped the 3 month follow-up CT to the planning CT. Hounsfield Unit differences (ΔHU) were extracted to assess lung parenchyma density changes. EQD2-ΔHU response was described sigmoidally, while regional response variation was studied by polar analysis. Prognostic factors of ΔHU were obtained through generalized linear modeling.

Results

Saturation of ΔHU was observed above 60 Gy. No interaction was found between boost dose distribution (D_{1cc} and V_{70Gy}) and ΔHU at lower doses. ΔHU was lowest peripherally from the tumor and peaked posteriorly at 3 cm from the tumor border (3.1 HU/Gy). Right lung location was an independent risk factor for ΔHU (p=0.02).

Conclusions

No apparent increase of lung density changes at 3 months follow-up was observed above 60 Gy EQD2 for NSCLC patients treated with (concurrent or sequential chemo) radiation. The mild response observed peripherally in the lung parenchyma might be exploited in plan optimization routines minimizing lung damage.

Introduction

Local recurrence rates in locally advanced non-small cell lung cancer (LA-NSCLC) remain high (30%) at 2 years after standard concurrent chemoradiotherapy. Also, overall survival rates are low (20%) at 5 years after treatment [1]. As higher prescribed radiation dose might be associated with increased long-term tumor control and survival, radiation dose-escalation strategies have been explored to improve outcome [2-3].

Recently, several planning studies and trials have embarked on dose-escalation using advanced treatment and imaging modalities [4-7]. One example is the phase II PET-boost trial based on the observation of residual metabolic-active tumor areas after therapy at locations corresponding with the original high uptake areas using a pre-treatment FDG-PET scan [4]. The trial randomizes between a non-selective boost to the whole primary tumor and a selective boost to the 50% SUV_{max} volume within the primary tumor [5]. In both study arms, an accelerated 24 fraction treatment is delivered, which may be combined with sequential or concurrent chemotherapy in case of stage III disease. Planned dose prescription is escalated until a limiting organ at risk (OAR) constraint is reached. It is uncertain whether these constraints safely apply to accelerated delivery of escalated doses. Therefore, next to the primary PET-boost trial objective to determine the freedom from local failure, a secondary objective is to thoroughly evaluate toxicities as a function of the dose and volume of tissue irradiated.

While the adopted pulmonary toxicity constraint (Mean Lung Dose (MLD) below 20 Gy), derived from historical conventionally fractionated treatments [8-9], appeared to work as intended in a hypofractionation setting [10], more in-depth analyses are still required to fully understand the impact of experimental dose-escalation treatments on pulmonary toxicity. In the PET-Boost trial, severe pulmonary toxicity events were acceptable in a preliminary analysis (9.5% grade$\geq$3 radiation pneumonitis) [11], however, the multifactorial nature of symptoms remains an important caveat [12]. Furthermore, pneumonitis symptoms are scored using graded non-quantitative scales (CTCAE 3.0), hampering dose response modeling. Therefore, image-based lung features could provide important additional information on lung damage, including voxelized response data of the lung parenchyma exposed to high dose. Understanding the regional dose volume effects responsible for lung parenchyma damage induction is a crucial step in order to be able to dissect the causes of the multifactorial radiation-induced pulmonary toxicity. One surrogate of lung damage is the lung tissue density change evaluated on CT scans. Indications that CT density changes indeed reflect lung tissue damage are its strong dose-dependence [13-23] and the correlation with pulmonary toxicity scores observed by some authors [20, 23]. This simple CT-based metric also proved to be a continuous and reproducible endpoint [15, 19-20].

Severe radiation-induced lung tissue damage occurs in approximately 20% of patients after standard treatment for LA-NSCLC [9,24-25]. The mechanism of formation of lung infiltrations is not well understood. Lung dose-density change models [15,19,22] could only be validated to a limited extent in individual patients or in subregions of the lung [20,26], and this mostly in stage I lesions treated with extreme hypofractionation, leading to a reproducible saturation of the dose response. A better understanding of the dose-density change response mechanism at the higher dose regimes in LA-NSCLC might be important for unraveling the causes of pulmonary toxicity and for increasing the therapeutic ratio using dose-escalation.

The aim of this study was to quantify early lung tissue CT density changes 3 months post-(chemo)radiotherapy in the PET-boost trial for LA-NSCLC, as a surrogate of lung damage. The possible impact of dose-volume features characterizing the high-dose lung tissue region was studied. Finally,

regional differences in lung density change were assessed and prognostic factors were searched through generalized linear modeling.

Methods and Materials

Patient dataset

The dataset consisted of 59 stage IB-III NSCLC patients treated after written informed consent in a randomized phase II study (NCT01024829), a PET-boost trial. PET-boost eligibility criteria included a minimum primary tumor (GTV_{prim}) diameter of 4 cm and no prior radiotherapy to the thorax. From 85 patients randomized between April 2010 and June 2015 in 3 institutions, 59 had a CT scan in the first 6 months after treatment. The study arms were a dose-escalation to the primary tumor planning target volume (PTV_{prim}) as a whole (Arm A), and an integrated boost to PTV_{high}, the expanded GTV_{high} (50% SUV_{max} volume of GTV_{prim}) (Arm B), both delivered in 24 fractions. Planned dose escalation was attempted until a limiting OAR constraint was reached. The highest allowed prescription dose was 129.6 Gy (5.4 Gy fraction dose). When constraints prevented escalation to at least 72 Gy (3 Gy fraction dose), the patient was treated with 66 Gy in 24 fractions and excluded from current analysis. Further planning details were previously described [5]. The planning CT (CT_0), follow-up CT (CT_{fup}) approximately 3 months post RT, contours and dose maps corrected to equivalent doses in 2 Gy fractions (EQD2, α/β=3 Gy [27]) were collected. Atelectasis on CT_0 was excluded from the lung contour.

Intensity-modulated radiotherapy (IMRT) or volumetric modulated arc therapy (VMAT) treatments were delivered. Mid-ventilation or mid-position planning CT scans were mostly used [28]. Free-breathing scans using an internal target volume approach were also accepted in the study (7 patients). Slice thickness was 3 mm and in-slice pixel size 0.98 mm.

No clinical target volume (CTV) margin was applied to GTV_{high}, while GTV_{prim} was enlarged by a CTV-margin of 0-5 mm. Patient-specific PTV margins of 10-15 mm were applied according to institutional policies accounting for various geometrical uncertainties such as delineation variability, differential motion between primary tumor and lymph nodes as well as respiratory motion. Advanced type B dose calculation algorithms were used, which consider lateral electron transport leading to accurate dose calculation near tissue inhomogeneities. Image guidance using daily cone beam CT (CBCT) was mandatory in the trial. CT_{fup} was an inspiration breath-hold scan in 35 patients and a mid-ventilation scan in 24 patients.

Density change analysis

Deformable Image Registration (DIR) mapped the CT_{fup} to the CT_0 using in-house developed software at XXXX. A multiresolution cubic B-spline algorithm (final control point spacing of 1 cm) driven by the Hounsfield Unit (HU) correlation ratio similarity measure was used [29]. Additional constraints on the smoothness and the rigidity of the deformation vector field within the 'both lungs minus GTV_{prim}' mask were used as regularization terms to avoid unnecessary reshaping of infiltrations on the CT_{fup} [30]. A rigid bony anatomy match was the starting point for the DIR. Subsequently, a dose–density change response analysis was performed in MeVisLab 2.6.2 (MeVis Fraunhofer, Bremen, Germany) as previously reported [20]. A difference image was created by voxel-wise subtraction of HU values ($\Delta HU = HU_{fup} - HU_0$). All voxels within the 'both lungs minus GTV_{prim}' mask, eroded by 1 voxel to eliminate potential errors at its boundary, were analyzed. For the overall dose response curve, the

dose map was first resampled to the CT image grid using Lanczos interpolation. Median ΔHU of lung voxels was extracted per dose bin of 5 Gy EQD2. Dose bins associated with a lung volume <10 cc were discarded on a per patient basis. For each patient, the median ΔHU in the lowest dose bin (lung voxels receiving <5 Gy) was subtracted from the median ΔHU of all other dose bins (i.e., negligible density change at low dose was assumed [13-14]). Sigmoids were fitted to the population average data points according to following logistic function,

$$\Delta\mathrm{HU} = \frac{\Delta\mathrm{HU}_{sat}}{1 + e^{4\gamma(1-\frac{D}{D_{50}})}}$$

with ΔHU_{sat} the ΔHU saturation level, D_{50} the dose where 50% of ΔHU_{sat} is reached and γ the steepness of the sigmoid. The saturation point was defined as the dose where 95% of ΔHU_{sat} was reached. For the regional dose response analysis, Lanczos resampling to a uniform 3 mm voxel grid was performed for ΔHU and dose maps. This way, representative one-voxel rings of ipsilateral lung ΔHU and dose at equal distances of 1, 2, 3 and 4 cm from the GTV_{prim} border could be selected in the central GTV_{prim} slice, in order to describe angular dose responses. Per ring and per patient, the median ΔHU and median ΔHU/Gy was defined per 20 degree angular bin (angles as seen from the GTV_{prim} center of mass). A zero degree angle referred to lung voxels located centrally from GTV_{prim}, while 90°, 180° and 270° indicated anterior, peripheral and posterior locations respectively. 6^{th} order polynomials were fitted to the average polar response data. All fits were performed in Matlab R2015b (The Mathworks Inc., Natick, MA) using least squares optimization.

Statistics

Differences in ΔHU response between study arms were analyzed using a Mann-Whitney U test for every dose bin. Prognostic factors of individual patients' ΔHU were searched in the representative 40-45 Gy, 60-65 Gy, 80-85 Gy and 100-105 Gy dose bins using univariate linear regression. The studied covariates were lung side, lobe location, central/peripheral tumor location, GTV_{prim} volume, prescription dose (EQD2), lung D_{1cc} (EQD2 delivered to hottest 1 cc of lung tissue), lung V_{70} (volume of lung receiving >70 Gy EQD2) as 70-75 Gy was the highest dose bin found in every patient, the mean lung dose (MLD), mean heart dose (MHD), heart D_{max}, chemotherapy regimen, age and treatment technique (VMAT vs IMRT). p-values below 0.05 were considered statistically significant. The False Discovery Rate (FDR) was controlled by the Benjamini-Hochberg procedure quantifying multiple testing error rates. Regional ΔHU was analyzed by comparing ΔHU of voxels located at the central, anterior, peripheral and posterior side of GTV_{prim} (detailed definition of these regions can be found in Appendix 1) in the 2 cm ring using within-subjects ANOVA with Fisher's LSD pairwise comparisons. Finally, a generalized linear model (GLM) was built separately for every covariate to test their interaction with regional location. All tests were performed in Statistica 13 (Dell Inc., Tulsa, OK).

Results

Patient and treatment characteristics are summarized in Table 1. The average ΔHU response data was well described sigmoidally (R^2=0.81) with model parameters D_{50}=29.9 Gy, ΔHU_{sat}=92.9 HU and γ=0.74. The saturation point was 60.0 Gy (Figure 1). Sigmoidal fits for the separate study arms were not statistically different according to the 95% confidence intervals of the model parameters (saturation points of 59.4 Gy and 66.8 Gy, Table 2) and no ΔHU difference between the study arms was observed in any of the dose bins (p>0.11). On the other hand, a likelihood ratio test indicated that the fit with separate sigmoids per study arm had a significantly higher likelihood (p<0.01). Lung D_{1cc} (higher in Arm A) had minimal non-local impact on ΔHU in lower dose bins, which was confirmed

in linear regression (non-significant negative associations between D_{1cc} and ΔHU). Appendix 2 shows the absence of any significant risk factor of ΔHU in linear regression.

The average angular ΔHU (radius at 2 cm from GTV_{prim}) was low peripherally from the tumor (approximately 50 HU) and peaked posteriorly and anterocentrally (100-150 HU) (Figure 2). The same behavior was observed in ΔHU/Gy analysis. Regional comparison identified a significantly lower ΔHU peripherally compared to centrally, p=0.050 (Table 3). Analyzing the average ΔHU as a function of distance from GTV_{prim}, it peaked centrally at 1 cm (183 HU), but peaked posteriorly at larger distances (167 HU at 3 cm). The peripheral response remained the lowest at all distances (between 53 HU and 64 HU). In ΔHU/Gy, the highest response was observed posteriorly at 3 cm (3.1 HU/Gy). It should be noted that most patients contributed only for a limited angle to this regional analysis according to the tumor location. In further GLM analysis, the central location could therefore not be included. An overview of primary tumor locations is depicted in Figure 3.

Taking regional differences into account in GLM modeling resulted in right lung as the only additional significant risk factor, with a large effect size (η^2): p=0.017 (FDR=22%) and η^2=0.39 for ΔHU and p=0.029 (FDR=38%) and η^2=0.34 for ΔHU/Gy. No indication of lung V_{70} or D_{1cc} causing ΔHU increase was thus observed. However, the D_{1cc} parameter was not equally distributed within its range as only a limited number of fraction doses >4 Gy and associated D_{1cc}>140 Gy were present in the dataset (Figure 3). Finally, combining lung side and D_{1cc} into one GLM resulted in regional location and lung side as independent predictors of ΔHU with p=0.035 (η^2=0.26) and p=0.028 (η^2=0.37), respectively (for ΔHU/Gy: p=0.024 (η^2=0.29) and p=0.045 (η^2=0.32), respectively).

Discussion

To the best of our knowledge this is the first study analyzing a quantitative endpoint of lung parenchyma damage on CT scan after dose-escalation treatments (>72 Gy in 24 fractions) for LA-NSCLC. We observed a saturation of lung dose-density response at biologically corrected doses >60 Gy EQD2 in IMRT or VMAT treated patients randomized in the PET-boost trial. The different boost techniques (including the whole primary tumor PTV or only a selected subvolume) did not influence the ΔHU feature, nor did the escalation volume or the highest dose level in the lung. No detrimental effect of a small high-dose lung region (D_{1cc} from 89.5 Gy EQD2 up to 245.9 Gy EQD2) on its local surrounding was observed. While dose-escalation was shown to be safe for clinical endpoints [11,31-32], our study confirms that prescribed doses from 86.4 Gy EQD2 to 217.7 Gy EQD2 (24 fractions of 3 Gy and 5.4 Gy, respectively) did not negatively impact an objective lung parenchyma density change endpoint 3 months post RT.

While local dose was strongly associated with local ΔHU response overall, subregion analysis brought more clarity to the mechanism of lung damage induction. Low ΔHU was reported for lung tissue located peripherally from the GTV_{prim} border, while the highest ΔHU/Gy response was observed in posterior direction. It should be noted that these findings relate only to a 2D analysis within the central tumor slice. A thorough 3D analysis in a larger dataset is required to understand the underlying cause. Finally, right-sided lungs showed significantly higher ΔHU independently of regional variations in our dataset.

Our results are consistent with literature. A lung tissue density increase plateau at 3 months was reported after stereotactic radiotherapy (SABR) of stage I tumors: above 80 Gy EQD2 [14], 30 Gy physical dose (equaling 63 Gy EQD2 for the predominant 4-fraction treatments) [13,18] or a patient-specific dose [20]. A saturation of lung perfusion reduction post SABR was also observed around 80

Gy EQD2 using SPECT scans [33]. After conventional LA-NSCLC treatments, likely due to lower lung doses rarely exceeding 60 Gy EQD2, a saturation could previously not be observed [15,17,20]. Regional differences in absolute ΔHU could not be explained by the regional heterogeneity of lung HU at baseline (heterogeneous presence of parenchyma, blood vessels and bronchial tree structure) as previously reported [20,26]. Peripheral lung tissue was not observed having lower baseline density in our dataset (Appendix 1, Figure A3). The remodeling of lung vasculature and subsequent pulmonary hypertension described after lung irradiation in small animal studies could be an explanation [34-35]. Pulmonary hypertension was shown to be associated with infiltrations located centrally in the lung, which corresponds to the higher density increase observed centrally compared to peripherally in our study [36]. Right-sided lungs were also previously reported to be prone to higher density increase [26]. It should be noted that slightly higher heart doses were delivered to right-sided tumors in our dataset. Nevertheless, the previously reported heart dose dependence of ΔHU could not be confirmed [37]. Similarly, no impact of chemotherapy regimen on ΔHU could be observed [22].

This study had some important limitations. The primary limitation was the challenging deformable registration of two CTs with 3 months interval, combined with tremendous tumor shrinkage, observed in almost all patients, and newly formed lung infiltrations. We designed a robust approach based on deformation field regularization and the assumption of elastic tumor regression, i.e., lung tissue surrounding the tumor moving inside the initial tumor volume [38]. Regularization term weights were optimized using a subset of the database by visual image overlay assessment of registrations. The optimized registration settings were then applied to all patients. In order to correct for the breathing state, a lung HU correction was also performed using the median ΔHU in the lung subvolume receiving 0-5 Gy. This median ΔHU in the low-dose region was considered a baseline breathing-related HU shift and thus subtracted from the median ΔHU of all other lung subvolumes. The validity of the underlying assumption of an undamaged low-dose region cannot be answered with this dataset. 4DCT acquisition is therefore recommended both for baseline and follow-up CT in future ΔHU response analyses. To limit potential errors in ΔHU quantification, additional safety measures were introduced. An erosion of the lung mask was performed to avoid potential boundary problems near the ribs (e.g. pleural effusion), GTV_{prim} (extreme tumor shrinkage), mediastinum and atelectasis regions. Regarding the latter, it should be noted that voxels within the atelectasis region on CT_0 were excluded from the lung contour and thus not included in our analysis. Finally, a minimal volume of 10 cc was required per dose bin and the median ΔHU over all bin voxels was computed to eliminate outliers. While these practices resulted in loss of some high-dose information, ΔHU up to 140 Gy EQD2 could be extracted (Figure 1). An unexplained drop in ΔHU was seen close to GTV_{prim} in several patients and was also visible in the Arm A response curve. Similar behavior was reported in other dose-density change studies [14,20,39]. Despite the safety measures, an influence of misregistrations centrally in the lung (mediastinum, large vessels, etc.) on the larger ΔHU observed centrally cannot completely be excluded. For the polar analysis, the median ΔHU over all voxels located within 20° sectors was computed with the same purpose of eliminating outliers. This limited angular resolution might have prevented the detection of effects associated with the different treatment dose accumulation history and dose rate variability of VMAT compared to IMRT treatments, potentially impacting lung damage. Nevertheless, the analysis of the standard deviation of ΔHU within the 20° sectors did not show any difference between IMRT and VMAT cases ($p>0.05$ for all sectors, Figure A4, Appendix 1). Taking into account the non-rigid registration uncertainties and the small VMAT cohort (14 patients), however, any difference in lung ΔHU response between both delivery techniques cannot be excluded based on this dataset.

Secondly, the limited size of the dataset prevented extensive multivariable analyses. For the same reason, the impact of only one dose (D_{1cc}) and volume (V_{70}) characteristic was analyzed, and FDR was introduced for multiple testing assessment. For the regional analysis, only few patients had lung tissue information for the whole 360° around GTV_{prim}, even at 1 cm distance. The number of cases with lung tissue located centrally from GTV_{prim} was quite limited (few small peripheral tumors, Figure 3). Patients that could not be escalated due to limiting OAR constraints were excluded from the study as it was a small (15 patients) and biased subgroup (e.g. large GTV volumes combined with the smallest lung volumes or highest heart doses). It should be noted that a large range of GTV_{prim} volumes (11-810 cc) was still present in our dataset.

Finally, we assumed planned dose to equal delivered dose during the whole time course of treatment. No adaptive re-planning was taken into our analysis, which could have been performed to account for intrathoracic anatomical changes. The different motion management techniques and margin concepts could also have influenced planned dose close to the tumor. Nonetheless, a ΔHU saturation was consistently observed in both treatment arms.

In summary, this study indicates that the induction of large lung density increase processes in LA-NSCLC treated with modern era IMRT and VMAT techniques is not influenced by high escalation doses to a small lung volume. The limited damage peripherally in the lung could be exploited by dose redistribution using IMRT optimization tools, proton therapy beam angle choices [40] or adaptive treatment workflows which have been shown to enable further dose-escalation [41-42]. At the same time, posteriorly located lung parenchyma could be spared especially in right-sided lungs by conformal avoidance planning. Importantly, the differential dose-ΔHU response between patients can be larger than the observed average regional differences, as indicated by a boxplot of all density changes in the dataset (Figure A5, Appendix 3). A genetic biomarker predicting the patient's lung damage susceptibility would therefore clearly improve the application of our findings. The clinical relevance of our strategies to limit lung damage should thus be validated in a clinical trial. Finally, future work should include more imaging features, to optimally capture different types of lung damage [43].

A time trend in lung density change response has been described previously [13, 15, 17]. Two phases could be unraveled: a transient phase peaking at 3-4 months and a fibrotic phase after 9 months. These were shown to coincide well with symptomatic radiation pneumonitis and fibrosis timepoints. The 3 month after treatment CT scan timepoint used in our study is thus representative for the early effect. This is a crucial timepoint as acute pulmonary toxicity was shown to be highly dose-limiting (e.g. in the QUANTEC dose response curves [8]). Moreover, the early effect was shown to be correlated to the late effect in an IMRT dataset [17]. On the other hand, a study in rats showed different pathologies involved in early and late radiation-induced lung damage and different dose volume dependences for the different timepoints [44]. Future time- and volume-dependent modeling efforts of CT derived damage metrics seem thus required. Additionally, studying other surrogates of lung damage based on functional lung ventilation or perfusion maps of the lung might be helpful, although initially unventilated/unperfused lung regions often recover after treatment, which might bias the lung dose-damage response modeling [45].

Present parenchyma lung density change findings could thus help in dissecting the causes of dose-limiting pulmonary toxicity. Lung damage is indeed likely to be an important driver of the multifactorial pulmonary toxicity endpoint, although reports on the coincidence of lung density changes with clinical symptoms have been inconsistent [19-20,23-24,32]. The new knowledge on ΔHU saturation and hotspot independence, together with lung side and regional variations, provides

crucial information explaining the variability in lung tissue dose-damage response and could thus lead to better understanding and prediction of pulmonary toxicity in future studies.

References

[1] Auperin A, Le Pechoux C, Rolland E, et al. Meta-analysis of concomitant versus sequential radiochemotherapy in locally advanced non-small-cell lung cancer. J Clin Oncol 2010;28:2181–90.

[2] XXXX

[3] Kong FM, Ten Haken RK, Schipper MJ, et al. High-dose radiation improved local tumor control and overall survival in patients with inoperable/ unresectable nonsmall- cell lung cancer: long term results of a radiation dose escalation study. Int J Radiat Oncol Biol Phys. 2005; 63: 324-333

[4] XXXX

[5] XXXX

[6] Cannon D, Mehta M, Adkison J et al. Dose-limiting toxicity after hypofractionated dose-escalated radiotherapyin non-small cell lung cancer. J Clin Oncol 2013; 31: 4343-8.

[7] Moller DS, Khalil AA, Knap MM, Muren LP, Hoffmann L. A planning study of radiotherapy dose escalation of PET-active tumour volumes in non-small cell lung cancer patients. Acta Oncol 2011; 50:883-8.

[8] Marks LB, Bentzen SM, Deasy JO et al. Radiation dose-volume effects in the lung. Int J Radiat Oncol Biol Phys 2010 ; 76: S70-76.

[9] XXXX

[10] XXXX

[11] XXXX

[12] Yirmibesoglu E, Higginson D, Fayda M et al. Challenges scoring radiation pneumonitis in patients irradiated for lung cancer. Lung Cancer 2012; 76: 350-3.

[13] XXXX

[13] Palma DA, van Sörnsen de Koste J, Verbakel W, Vincent A, Senan S. Lung density changes after stereotactic radiotherapy : a quantitative analysis in 50 patients. Int J Radiat Oncol Biol Phys 2011; 81: 974-8.

[14] Diot Q, Kavanagh B, Schefter T, Gaspar L, Stuhr K, Miften M. Regional normal lung tissue density changes in patients treated with stereotactic body radiation therapy for lung tumors. Int J Radiat Oncol Biol Phys 2012; 84: 1024-30.

[15] Diot Q, Marks L, Bentzen S et al. Comparison of radiation-induced normal lung tissue density changes for patients from different institutions receiving conventional or hypofractionated treatments. Int J Radiat Oncol Biol Phys 2014; 89: 626-32.

[16] Bertelsen A, Schytte T, Bentzen SM, Hansen O, Nielsen M, Brink C. Radiation dose response of normal lung assessed by Cone Beam CT – A potential tool for biologically adaptive radiation therapy. Radiother Oncol 2011; 100: 351-5.

[17] Bernchou U, Schytte T, Bertelsen A, Bentzen SM, Hansen O, Brink C. Time evolution of regional CT density changes in normal lung after IMRT for NSCLC. Radiother Oncol 2013; 109: 89-94.

[18] Vinogradskiy Y, Diot Q, Kavanagh B, Schefter T, Gaspar L, Miften M. Spatial and dose-response analysis of fibrotic lung changes after stereotactic body radiation therapy. Med Phys 2013; 40: 081712.

[19] XXXX

[20] XXXX

[21] Ghobadi G, Wiegman EM, Langendijk JA, Widder J, Coppes RP, van Luijk P. A new CT-based method to quantify radiation-induced lung damage in patients. Radiother Oncol 2015; 117: 4-8.

[22] XXXX

[23] Wennberg B, Gagliardi G, Sundbom L, Svane G, Lind P. Early response of lung in breast cancer irradiation : radiologic density changes measured by CT and symptomatic radiation pneumonitis. Int J Radiat Biol Phys 2002; 52: 1196-1206.

[24] Moiseenko V, Craig T, Bezjak A, Van Dyk J. Dose-volume analysis of lung complications in the radiation treatment of malignant thymoma : a retrospective review. Radiother Oncol 2003; 67: 265-74.

[25] XXXX

[26] XXXX

[27] Jone B, Dale R, Deehan C, Hopkins K, Morgan D. The role of biologically effective dose (BED) in clinical oncology. Clin Oncol 2001; 13: 71-81.

[28] XXXX

[29] XXXX

[30] Staring M, Klein S, Pluim JPW. A rigidity penalty term for nonrigid registration. Med Phys 2007; 34: 4098.

[31] Partridge M, Ramos M, Sardaro A, Brada M. Dose escalation for non-small cell lung cancer: Analysis and modelling of published literature. Radiother Oncol 2011; 99: 6-11.

[32] Kong F-M, Hayman JA, Griffith KA et al. Final toxicity results of a radiation-dose escalation study in patients with non-small cell lung cancer (NSCLC) : predictors for radiation pneumonitis and fibrosis. Int J Radiat Oncol Biol Phys 2006; 65: 1075-86.

[33] XXXX

[34] Novakova-Jiresova A, van Luijk P, van Goor H, et al. Changes in expression of injury after irradiation of increasing volumes in rat lung. Int J Radiat Oncol Biol Phys 2007; 67: 1510-8.

[35] Ghobadi G, Bartelds B, van der Veen S et al. Lung irradiation induces pulmonary vascular remodelling resembling pulmonary arterial hypertension. Thorax 2012; 67: 334-41.

[36] McCann C, Gopalan D, Sheares K, Screaton N. Imaging in pulmonary hypertension, part 1: clinical perspectives, classification, imaging techniques and imaging algorithm. Postgrad Med J 2012; 88: 271-9.

[37] Cella L, D'Avino V, Palma G et al. Modeling the risk of radiation-induced lung fibrosis : Irradiated heart tissue is as important as irradiated lung. Radiother Oncol 2015; 117: 36-43.

[38] XXXX

[39] Jijo P, Yang C, Wu H et al. Early assessment of treatment responses during radiation therapy of lung cancer based on quantitative analysis of daily CT. Int J Radiat Oncol Biol Phys 2017; 98: 463-72.

[40] Zhang X, Li Y, Pan X et al. Intensity-modulated proton therapyreduces the dose to normal tissue compared with intensity-modulated radiation therapy or passive scattering proton therapy and enables individualized radical radiotherapy for extensive stage IIIB non-small cell lung cancer: a virtual clinical study. Int J Radiat Oncol Biol Phys 2010; 77: 357-66.

[41] Guckenberger M, Wilbert J, Richter A, Baier K, Flentje M. Potential of adaptive radiotherapy to escalate the radiation dose in combined radiochemotherapy for locally advanced non-small cell lung cancer. Int J Radiat Oncol Biol Phys 2011; 79: 901-8.

[42] XXXX

[43] Bernchou U, Christiansen RL, Asmussen JT, Schytte T, Hansen O, Brink C. Extent and computed tomography appearance of early radiation induced lung injury for non-small cell lung cancer. Radiother Oncol 2017; 123: 93-8.

[44] van der Veen SJ, Faber H, Ghobadi G et al. Decreasing irradiated rat lung volume changes dose-limiting toxicity from early to late effects. Int J Radiat Oncol Biol Phys 2016; 94: 163-71.

[45] Seppenwoolde Y, Muller S, Theuws J. Radiation dose-effect relations and local recovery in perfusion for patients with non-small-cell lung cancer. Int J Radiat Oncol Biol Phys 2000; 47: 681-90.

Figure captions

Figure 1. Population dose response curves for local density change of lung tissue 3 months post treatment.

In the whole dataset of 59 patients *(left graph)* and separately for Arm A (28 patients, non-selective boost) and Arm B (31 patients, selective boost) of the PET-boost trial *(right graph)*. Mean and standard error of mean (SEM) per 5 Gy dose bin and sigmoidal fit to the data points (least squares optimization using the reciprocals of SEM as weights). Model parameters of the fits are summarized in Table 2. The saturation point (dose where 95% of the saturation level ΔHU_{sat} is reached) is indicated on the curves by a cross mark.

Figure 2. Polar plot of lung tissue density changes 3 months post treatment.

Median ΔHU and ΔHU/Gy of all lung voxels in the same angular location from the primary tumor GTV center of mass perspective, averaged over all patients. Lung voxels in rings at 1, 2, 3 and 4 cm distance from the primary tumor GTV boundary were combined per 20 degree angular bins and 6^{th} order polynomials provided the best fit to the data points. Peripherally (towards the thoracic wall) very small changes were observed. At larger distances from the tumor, the highest density change was observed posteriorly. The average lung tissue doses delivered per angle can be found in Appendix 1 (Figure A2).

Figure 3. Overview of tumor locations and prescription doses.

Center of mass location of the primary tumors in the dataset *(left figure)*. Radiological convention views of the 59 center of mass coordinates transferred to a reference lung. Overview of the prescribed fraction doses in the dataset and the associated lung tissue D_{1cc} (EQD2 to hottest 1 cc of lung tissue) planned *(right figure)*. The fraction doses ranged from a lower limit of 3 Gy (1 patient) to an upper limit of 5.4 Gy (5 Arm B patients). All treatments were delivered in 24 fractions.

Table

Table 1 Patient and treatment characteristics of the 59 analyzed PET-boost trial patients. Descriptive statistics, variables are summarized by median value and range, or absolute number and percentage.

	n=59
Gender	
Male	44 (74.6%)
Female	15 (25.4%)
Age (years)	69.3 (36.2-83.9)
Chemotherapy treatment	
Concurrent	39 (66.1%)
Sequential	5 (8.5%)
None	15 (25.4%)
Lung side	
Right	36 (61.0%)
Left	23 (39.0%)
Lung lobe	
Upper	37 (62.7%)
Lower	18 (30.5%)
Combined	4 (6.8%)
Treatment technique	
IMRT	45 (76.3%)
VMAT	14 (23.7%)
Study arm	
Arm A	28 (47.5%)
Arm B	31 (52.5%)
GTV_{prim} volume (cc)	113.8 (11.0-809.7)
Prescribed dose (Gy EQD2)	
Arm A	101.7 (86.4-177.0)
Arm B	108.6 (90.6-217.7)
Mean Lung Dose (Gy physical dose)	17.9 (7.8-22.0)
Mean Heart Dose (Gy physical dose)	11.3 (0.5-34.1)
Heart D_{max} (Gy EQD2)	80.0 (1.3-111.2)
Lung D_{1cc} (Gy EQD2)	113.5 (89.5-245.9)
Lung V_{70} volume (cc)	172.1 (70.9-526.0)
CT_{fup} timepoint (months)	2.9 (0.4-4.1)
Dose voxel size (mm)	3.0 (2.5-4.0)

Abbreviations: IMRT: Intensity-Modulated Radiotherapy; VMAT: Volumetric Modulated Arc Therapy; GTV_{prim}: primary Gross Tumor Volume; EQD2: Equivalent Dose in 2 Gy fractions; Lung D_{1cc}: Minimal lung dose of hottest 1cc of lung; Lung V_{70}: Relative lung volume receiving at least 70 Gy; CT_{fup}: Follow-up CT scan.

Table 2 Model parameters D_{50}, ΔHU_{sat} and γ of the sigmoidal fits to the population average EQD2-ΔHU data points. Optimal fit parameters and 95% confidence interval (profile likelihood method) for the whole dataset and separately for patients treated in both study arms. No significant difference between the fits was found according to 95% CI of the parameters. The last column describes the global fit quality assessed using the coefficient of determination (R^2). Figure 1 depicts the corresponding sigmoids and data points.

	D_{50} (Gy)	ΔHU_{sat} (HU)	γ	R^2
Whole dataset (n=59)	29.9 (25.8; 33.9)	92.9 (74.3; 111.4)	0.74 (0.37; 1.11)	0.81
Arm A (n=28)	30.4 (26.8; 34.0)	90.2 (74.4; 106.0)	0.78 (0.42; 1.14)	0.79
Arm B (n=31)	32.2 (25.5; 38.9)	102.3 (65.6; 138.9)	0.69 (0.17; 1.20)	0.81

Abbreviations: D_{50}: Dose where 50% of maximal dose response (ΔHU_{sat}) is reached; Gy: Gray; HU: Hounsfield Units; ΔHU_{sat}: the saturation level of ΔHU response; γ: Steepness of the dose response sigmoid; R^2: Coefficient of determination.

Table 3 Regional differences in lung tissue density change between 4 distinct lung locations in a ring at 2 cm distance around the primary tumor GTV. The 2 cm ring was chosen for regional comparisons as its dose is not consistently exceeding the saturation point (as opposed to rings at shorter distance, Appendix 1 (Figure A2)), and as it contains a large number of lung voxels around the primary tumor (as opposed to rings at larger distances). Pairwise comparison p values (Fisher's LSD test) of a within-subjects ANOVA and mean difference and 95% confidence interval (CI) for the ΔHU and ΔHU/Gy metrics. Significant differences in bold.

	ΔHU		ΔHU/Gy	
	p	Mean difference and 95% CI (HU)	p	Mean difference and 95% CI (HU/Gy)
Peripheral vs Central	**0.050**	**-161.5 (-323.5;0.47)**	0.056	-1.77 (-3.62;-0.079)
Peripheral vs Posterior	0.074	-137.5 (-299.5;24.5)	0.068	-1.63 (-3.47;0.22)
Peripheral vs Anterior	0.12	-109.5 (-271.5;52.5)	0.12	-1.25 (-3.10;0.59)
Posterior vs Central	0.67	-24.0 (-186.0;138.0)	0.82	-0.14 (-1.99;1.70)
Posterior vs Anterior	0.62	28.0 (-134.0;190.0)	0.57	0.37 (-2.22;1.48)
Central vs Anterior	0.38	52.0 (-110.0;214.0)	0.44	0.51 (-1.33;2.36)

Abbreviations: HU: Hounsfield Units; CI: Confidence Interval; Gy: Gray.

Figure 1

Click here to download high resolution image

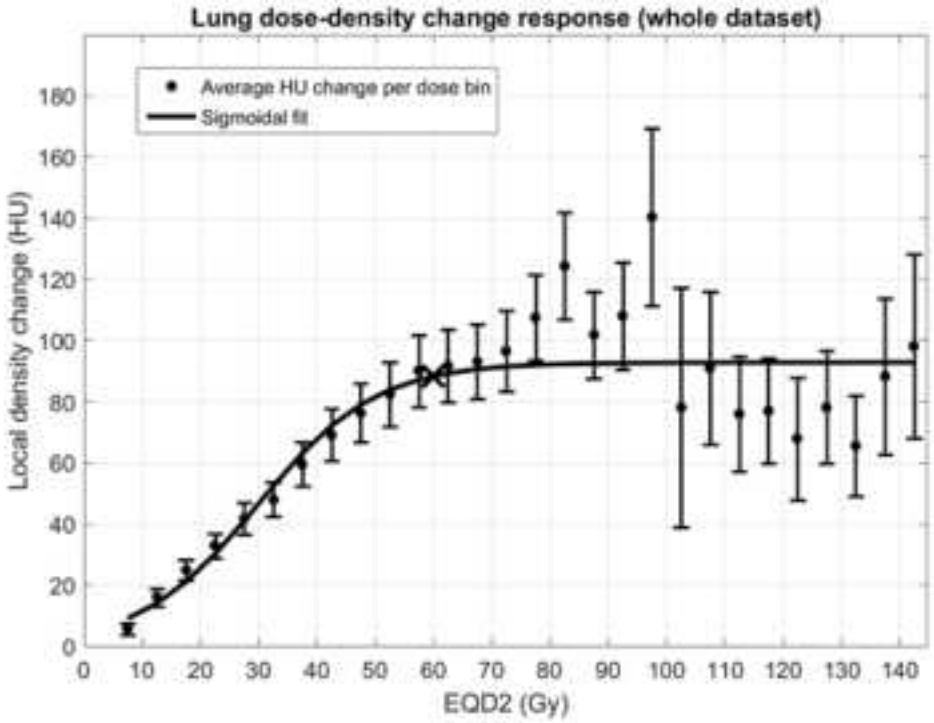

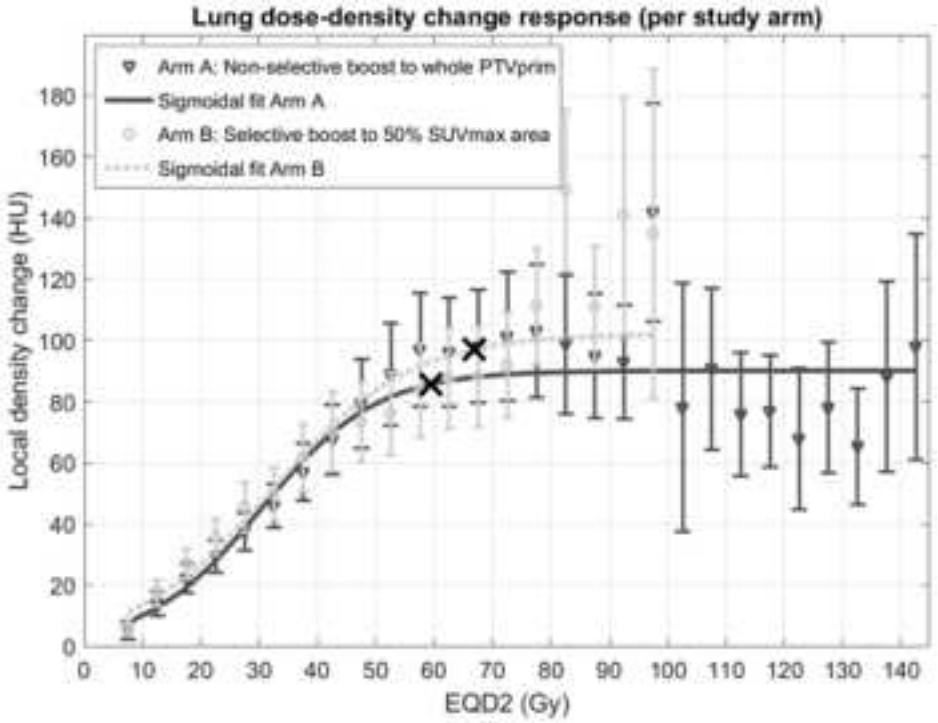

Figure 2

Click here to download high resolution image

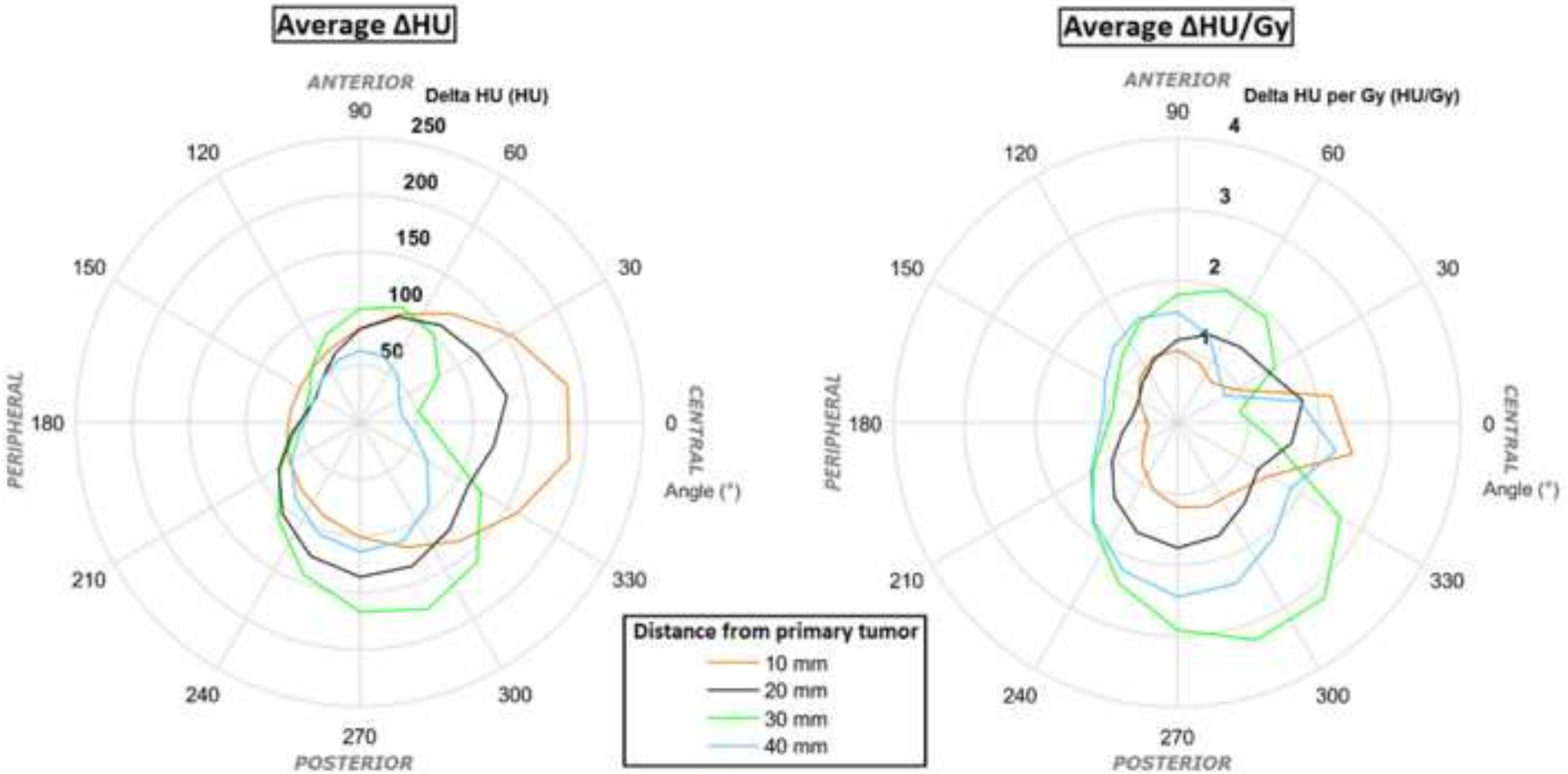

Figure 3

Click here to download high resolution image